CHEMISTRY OF MATERIALS

pubs.acs.org/cm

Article

Pulsed Laser Deposition of $Cs_2AgBiBr_6$: from Mechanochemically Synthesized Powders to Dry, Single-Step Deposition

Nathan Rodkey, Stan Kaal, Paz Sebastia-Luna, Yorick A. Birkhölzer, Martin Ledinsky, Francisco Palazon, Henk J. Bolink, and Monica Morales-Masis*

Cite This: *Chem. Mater.* 2021, 33, 7417–7422

Read Online

ACCESS | Metrics & More | Article Recommendations | Supporting Information

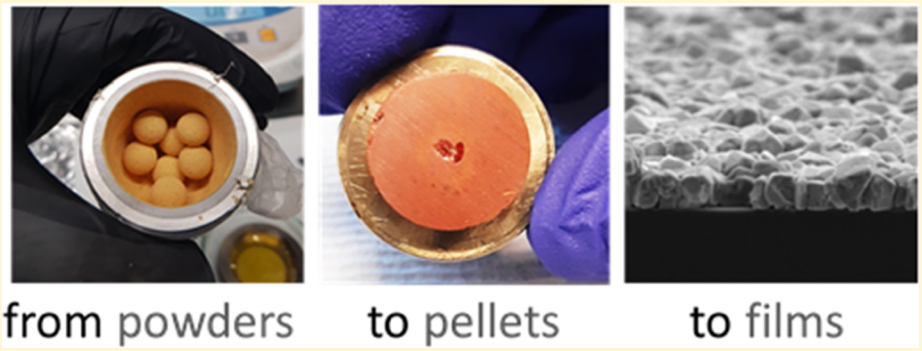

ABSTRACT: $Cs_2AgBiBr_6$ has been proposed as a promising lead-free and stable double perovskite alternative to hybrid and lead-based perovskites. However, the low solubility of precursors during wet synthesis, or the distinct volatility of components during evaporation, results in complex multistep synthesis approaches, hampering the widespread employment of $Cs_2AgBiBr_6$ films. Here, we present pulsed laser deposition of $Cs_2AgBiBr_6$ films as a dry, single-step and single-source deposition approach for high-quality film formation. $Cs_2AgBiBr_6$ powders were prepared by mechanochemical synthesis and pressed into a solid target maintaining phase purity. Controlled laser ablation of the double perovskite target in vacuum and a substrate temperature of 200 °C results in the formation of highly crystalline $Cs_2AgBiBr_6$ films. We discuss the importance of deposition pressure to achieve stoichiometric transfer and of substrate temperature during PLD growth to obtain high-quality $Cs_2AgBiBr_6$ films with grain sizes > 200 nm. This work demonstrates the potential of PLD, an established technique in the semiconductor industry, to deposit complex halide perovskite materials while being compatible with optoelectronic device fabrication, such as UV and X-ray detectors.

I. INTRODUCTION

Double halide perovskites, of the form $A_2M'M''X_6$, have emerged as promising alternatives to hybrid and lead-based halide perovskites due to their stability and promising optoelectronic properties for photo- and X-ray detectors,[1] light-emitting diodes (LEDs),[2] and wide-band-gap solar cells.[3,4] This double perovskite structure has opened opportunities to explore a broad composition space, for example, the computational chemistry side of perovskite materials with an estimated 9520 combinations of halide double perovskites, many of them remain unsynthesized. Out of these many possible combinations,[5] $Cs_2AgBiBr_6$ stands out as the most widely studied and archetypical double perovskite. As such, many groups have been looking into derivatives of the $Cs_2AgBiBr_6$ compound[6,7] or doping[4] to tune its properties for use as possible photovoltaic (PV) absorbers, light emitters, or photodetectors.

The synthesis of these multicompound materials (usually containing four or more elements) in the thin-film form has proven to be challenging. Most reports on double perovskites have focused on nanocrystals[8−11] or solution-based processes where powders are obtained through a filtering and drying process.[12−14] Specifically for $Cs_2AgBiBr_6$, only few studies have shown thin films of double perovskites formed through the traditional spin-coating process,[3,15,16] where low solubility of precursors hampered the synthesis of dense, thick films.[15,17,18] In this respect, dry, vapor-based processes are preferred for $Cs_2AgBiBr_6$.[19,20] Sequential evaporation, coevaporation, and single-source evaporation have been employed to deposit $Cs_2AgBiBr_6$ films; however, postannealing processes are required to achieve or improve the phase purity.[19,20]

In this work, we demonstrate that pulsed laser deposition (PLD) allows for the single-source, near-stoichiometric

Received: June 15, 2021
Published: September 6, 2021

https://doi.org/10.1021/acs.chemmater.1c02054
Chem. Mater. 2021, 33, 7417–7422

transfer from a solid $Cs_2AgBiBr_6$ target to $Cs_2AgBiBr_6$ films. This is possible due to a nonequilibrium ablation of the solid target with an excimer laser[21] and after careful tuning of deposition parameters. In particular, PLD shows extensive promise in photodetector and laser diode applications where highly controlled and highly crystalline (at times epitaxial) growths are required. Below we describe the importance of the PLD optimization process, with a focus on the effect of pressure and substrate temperature to achieve both, near-stoichiometric transfer of $Cs_2AgBiBr_6$-pressed powders into thin films and high film crystallinity in a single-step process.

II. METHODS

$Cs_2AgBiBr_6$ powders were first synthesized by mechanochemical grinding (i.e., ball milling)[22] of stoichiometric ratios of CsBr, AgBr, and $BiBr_3$ powders purchased from TCI, Alfa Aesar, and Sigma-Aldrich, respectively. These powders were then pressed uniaxially with a pressure of ∼600 MPa for 30 min to form a thick, disc-shaped target, 20 mm in diameter. The deposition of thin films by PLD was performed using a Coherent KrF excimer laser (λ = 248 nm) to ablate the solid target under vacuum in an Ar atmosphere (various working pressures described in Section III). The ablation took the form of a 4 × 4 mm^2 scan, with subsequent ablations (for more thin-film depositions) done on "fresh," unablated parts of the pressed target. Pre- and postablation analyses of the target via energy-dispersive X-ray spectroscopy (EDX) (Figure S1) indicate no change of the target composition after ablation. As ablation spots are only few micrometers in depth, to reuse the target, the top surface is grinded down using a fine sandpaper. This allows for multiple depositions from a single pellet. A target-to-substrate distance of 60 mm was used and the substrate temperature was varied between room temperature (RT) and 200 °C. For all samples, unless otherwise stated, a laser fluence of 0.45 J/cm^2, frequency of 8 Hz, and 1 mm^2 spot size were used, which led to deposition rates of ∼4.3 nm/min. Silicon (100) substrates with a native oxide layer were used to characterize films by X-ray diffraction (XRD), while fused-silica substrates were used for optical analysis. XRD measurements were done in a symmetric configuration using a PANalytical X'Pert PRO with a Cu anode X-ray source. A Perkin Elmer UV−vis−NIR spectrophotometer was used to measure absorbance. The photoluminescence (PL) measurement was excited with a 442 nm laser (Renishaw inVia Reflex micro spectrometer). The response calibration was applied during the measurement to reveal the real shape of the luminescence spectra. Photothermal deflection spectroscopy (PDS) was used to measure the optical absorption of thin films with high sensitivity at a broad spectral range of 400−1000 nm. The deflection of a probe laser beam directly determines the quantity of absorbed light via sample thermal changes.

III. RESULTS AND DISCUSSION

III.I. Mechanochemical Synthesis of $Cs_2AgBiBr_6$ Powders and Solid Pellets. CsBr, AgBr, and $BiBr_3$ powders were mixed in 2:1:1 molar ratios. The estimated mass fractions of different phases formed at each stage (derived from Rietveld refinements of powder XRD data; see Figure S2) are presented in Figure 1a.

As seen in Figure 1a, binary precursors react very rapidly in the first few minutes. Nevertheless, the significant fraction of two different Cs−Bi−Br phases, namely, Cs_3BiBr_6 and $Cs_3Bi_2Br_9$ at t < 15 min, as well as the remaining AgBr (estimated residual mass fraction of 2.7% after 1 h of milling), suggests that the reaction proceeds preferentially in several steps, with an initial reaction between CsBr and $BiBr_3$, followed by the slower incorporation of AgBr. A plausible reaction mechanism based on this data is as follows

$$3\ CsBr + BiBr_3 \rightarrow Cs_3BiBr_6 \quad (1)$$

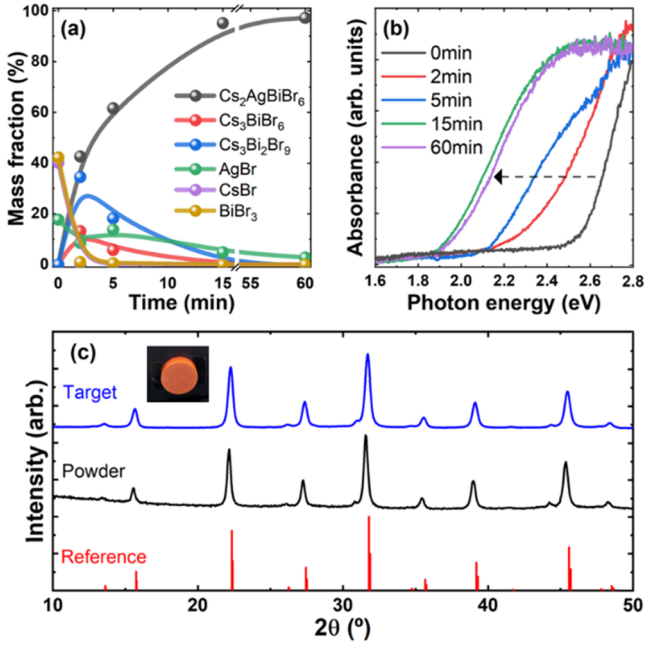

Figure 1. (a) Mass fraction of different phases present after varying ball-milling times, derived from Rietveld refinements of powder XRD data (Figure S3). CsBr line overlaps very closely that of $BiBr_3$ and is therefore barely noticeable. (b) Absorbance spectra of samples ball-milled for different times. (c) XRD data of powder (black line) and target (blue line) samples as well as the $Cs_2AgBiBr_6$ reference pattern (ICSD 18989). Picture of the pressed $Cs_2AgBiBr_6$ target in the inset.

$$Cs_3BiBr_6 + BiBr_3 \rightarrow Cs_3Bi_2Br_9 \quad (2)$$

$$Cs_3Bi_2Br_9 + 2\ AgBr + CsBr \rightarrow 2\ Cs_2AgBiBr_6 \quad (3)$$

To completely elucidate different and potentially complex reaction mechanisms at play, a more detailed analysis at shorter time intervals (t < 2 min) would certainly be needed, but this is beyond the scope of this work. On the contrary, it is worth noting that at a relatively short milling time of 15 min the sample consists of nearly phase-pure $Cs_2AgBiBr_6$ and remains so after milling for longer times up to 1 h. Optical absorption measurements (Figure 1b) confirm the reaction kinetics observed by XRD. Indeed, the starting powder is transparent below 2.6 eV, which is in line with the reported band gaps of AgBr and $BiBr_3$ (that of CsBr being wider).[23,24] Upon milling, the absorption red-shifts until reaching a stable onset around 1.95 eV, in accordance with the reported values for $Cs_2AgBiBr_6$.[25] For intermediate ball-milling times (t = 2 and 5 min), the absorption onset is found within 2.3 and 2.1 eV. While it is tempting to attribute this to the aforementioned intermediate species Cs_3BiBr_6 and $Cs_3Bi_2Br_9$, these are actually reported to have wider band gaps.[26−28] Hence, it is more reasonable to ascribe this absorption to the already-present fraction of $Cs_2AgBiBr_6$ at these intermediate times (40−60% in mass approximately; see Figure 1a). Indeed, band gap values ranging from 1.9 to 2.2 eV have been reported for this material.[4,29] Furthermore, this is also known to vary with structural (dis)order, which could be affected by ball milling.[29,30] Figure 1c displays the XRD pattern of mechanochemically synthesized $Cs_2AgBiBr_6$ powders and the corresponding solid target. Both patterns follow the $Cs_2AgBiBr_6$ reference (ICSD 18989), indicating no degradation of the phase after uniaxial pressing.

https://doi.org/10.1021/acs.chemmater.1c02054
Chem. Mater. 2021, 33, 7417−7422

III.II. Pulsed Laser Deposition of $Cs_2AgBiBr_6$ Films from $Cs_2AgBiBr_6$ Solid Pellets. One of the known advantages of PLD is the possibility to achieve near-stoichiometric transfer of multicompound materials.[31,32] However, this requires careful optimization of parameters such as pressure, laser fluence, and target-to-substrate distance. Based on previous reports,[33] a laser fluence of 0.45 J/cm^2 and a substrate to target distance of 60 mm were selected. The effects of pressure and substrate temperature on the stoichiometric transfer and high-crystalline quality are described below.

III.II.I. Effect of Deposition Pressure. During PLD, the plume shape and energetics of the ablated particles arriving at the substrate are strongly influenced by the deposition pressure.[25,26] At low pressures, the ablated species experience little scattering, arriving at the surface of the substrate with a large portion of their initial kinetic energy. In this way, sputtering of the surface may occur, often preferentially.[34] At higher pressures, more scattering ensues and ablated species are thermalized (i.e., their kinetic energy resembles that of the background gas). To investigate the influence of deposition pressure during PLD from a $Cs_2AgBiBr_6$ target, we have grown films at different pressures, tuned via the introduction of Ar gas in the chamber. Figure 2a displays the XRD patterns of films

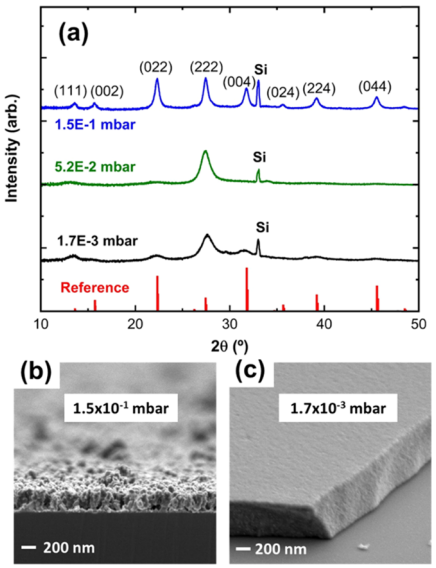

Figure 2. (a) Thin films grown at room temperature with deposition pressures of 1.7 × 10^{-3}, 5.2 × 10^{-2}, and 1.5 × 10^{-1} mbar. While the (222) plane of $Cs_2AgBiBr_6$ is visible at all deposition pressures, EDX indicates excesses of Ag in the film deposited at 1.7 × 10^{-3} mbar. Only at a deposition pressure of 1.5 × 10^{-1} mbar was the growth of a distinct $Cs_2AgBiBr_6$ phase observed. SEM cross sections of samples deposited at (b) 1.5 × 10^{-1} and (c) 1.7 × 10^{-3} mbar show the transition from dense (low deposition pressure) to porous films (high deposition pressures).

grown at three distinct pressures: 1.7 × 10^{-3}, 5.2 × 10^{-2}, and 1.5 × 10^{-1} mbar. We observe that, with increasing deposition pressure, the films begin to resemble the XRD reference of cubic $Cs_2AgBiBr_6$. At low pressures (1.7 × 10^{-3} and 5.2 × 10^{-2} mbar), the films are highly dense (Figure 2c), but only show a wide (222) peak, which may be the result of embedded $Cs_2AgBiBr_6$ growths in an amorphous matrix. At 1.7 × 10^{-3} mbar in particular, evidence of excess silver was verified by EDX (Figure S4) and visualized by scanning electron microscopy (SEM). Through a series of annealing steps, the growth of silver-rich particles on the surface of annealed samples at 230 and 280 °C was observed, as shown in Figure S5. Increasing the pressure to 5.2 × 10^{-2} mbar caused no pronounced effect on the film microstructure; however, further increasing the deposition pressure to 1.5 × 10^{-1} mbar led to the growth of a film with a distinct $Cs_2AgBiBr_6$ phase. EDX analysis of films grown at this pressure and 200 °C substrate temperature will be described in the next section. While the $Cs_2AgBiBr_6$ phase is achieved at high deposition pressures, the high pressure has a side effect on the microstructure, i.e., porosity, as observed in the cross-sectional SEM images in Figure 2b. This is a well-known phenomenon in physical vapor deposition growths and is described further on.

The link between deposition pressure, thermalization, and stoichiometric transfer can be described following a model proposed by Westwood[35] and summarized in the Supporting Information. Following this model, the distance required for each ablated species to thermalize as a function of the deposition pressure can be estimated. Figure 3 shows the

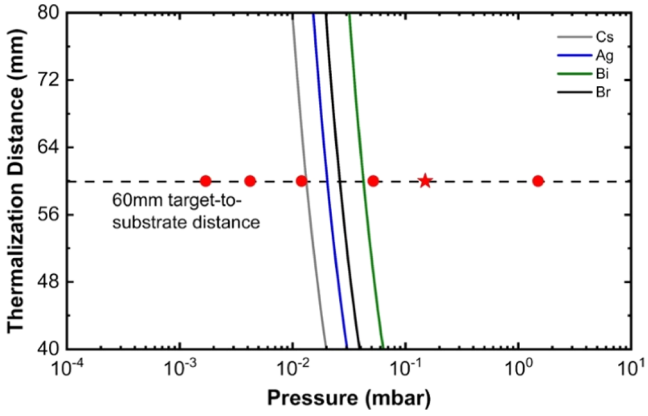

Figure 3. Thermalization distance as a function of the Ar background gas pressure following a model by Westwood.[35] The target-substrate distance used in this work is 60 mm and is denoted by a dashed line. The closed red circles note growth conditions used where phase-pure growth was not observed. The star, at 1.5 × 10^{-1} mbar, denotes the nearly phase-pure growth of $Cs_2AgBiBr_6$ films.

resulting estimates (solid lines) for the elements Cs, Ag, Bi, and Br. The red circles denote experimental points (i.e., films grown at specific deposition pressures) at which no phase-pure growth was observed, while stars denote single-phase growth. Only once the estimated thermalization point of all constituent elements is breached a single-phase growth is observed. As noted, films were grown at 1.5 mbar showed no phase-pure growth while being well above the estimated thermalization region. One possible explanation is that at very high pressures, preferential scattering of lighter atoms occurs affecting the final stoichiometry of the film.[34] Based on this analysis and the results presented in Figure 2, we propose an ideal pressure range between 0.1 and 1 mbar for thermalization of the Cs–Ag–Bi–Br species and near-stoichiometric transfer from the target to the film to occur. Note that this conclusion might vary with materials and specific PLD parameters used.

One strategy to alleviate the pressure-dependence of these growths is through the introduction of excess elements (usually the most volatile) in the source material, as has been shown for other single-source processes and/or materials deposited by either PLD or evaporation.[36,37]

https://doi.org/10.1021/acs.chemmater.1c02054
Chem. Mater. 2021, 33, 7417–7422

III.II.II. Effect of Substrate Temperature. As observed in Figure 2, room-temperature depositions of $Cs_2AgBiBr_6$ result in porous films, and therefore, to improve the films morphology, the effect of substrate temperature was evaluated. The XRD patterns of room temperature versus 200 °C growths are shown in Figure 4a, with the drastic increase in crystallinity

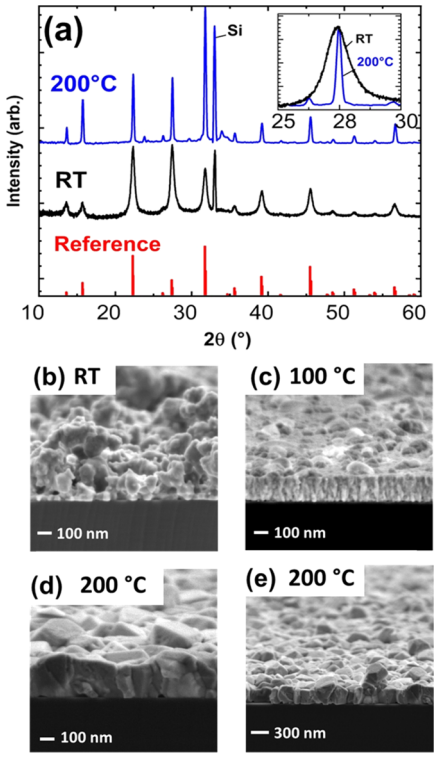

Figure 4. $Cs_2AgBiBr_6$ thin films grown at a deposition pressure of 1.5×10^{-1} mbar and different substrate temperatures. (a) Side-by-side comparison of XRD patterns for $Cs_2AgBiBr_6$ films grown at room temperature (RT) and 200 °C, both showing the double perovskite phase. Inset: zoomed in the (002) plane showing clear sharpening of the peak with increasing growth temperatures, i.e., improvement in crystallinity. Panels (b–d) show the film morphology progression from RT, 100 °C, and 200 °C growths, respectively. Films deposited at 200 °C show grains sizes of ∼300 nm, with (e) showing a zoomed-out view of a 200 °C growth to better evaluate film morphology.

noticeable in the shrinking XRD peak width (inset of Figure 4a) for films grown at 200 °C, and by cross-sectional SEM images (Figure 4b–e). The composition of the films was verified by EDX, showing mean atomic percentages of 21% Cs, 11% Ag, 9% Bi, and 59% Br (statistics in Table S6). The statistical mean shows a near-stoichiometric thin film with a possible bismuth deficiency but remains within a range of error of EDX measurements.

The improved film density and crystalline growth with increased substrate temperature can be described with the Thornton model,[38] a model typically employed for physical vapor deposition of inorganic materials. This model describes the transition in crystallization regimes as a function of its background gas pressure and substrate temperature. At low temperatures, surface diffusion is limited, and the growth is dominated by shadowing effects, introducing porosity into the system (Figure 4b). As the temperature is increased, the added energy allows for surface diffusion to take over. However, atoms are unlikely to diffuse between crystallites and with growth limited to the surface, columnar-like structures are formed (Figure 4c). Finally, at even higher temperatures, bulk recrystallization processes gain enough energy to occur, coalescing the crystallites during the growth to form large grains (Figure 4d). For the growth of $Cs_2AgBiBr_6$ at 1.5×10^{-1} mbar, these transitions correspond to room temperature, 100 °C, and 200 °C growths, as shown in Figure 4b–e. Unique to PLD, we note that the laser fluence can also be tuned to transition from porous to dense films, respectively (Figure S7), but we refrain from using high values of fluence (1.61 J/cm^2) due to possible damage to the target during ablation.

Once the growth was optimized, we verified the optical properties of ∼200 nm thick films, grown at 200 °C, through absorbance, PL, and PDS (Figure 5a,b). Notably, we report a

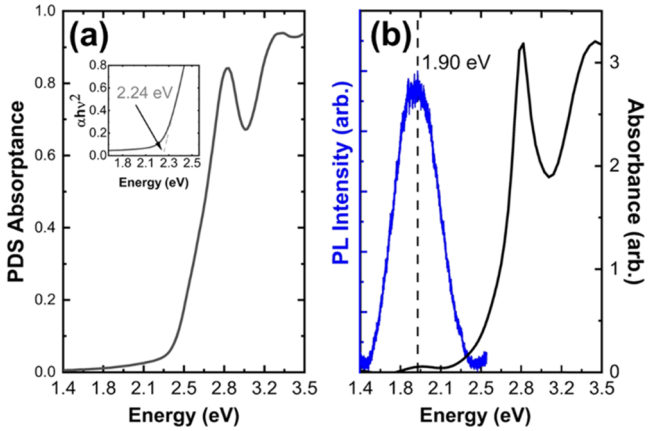

Figure 5. Optical measurements performed on 200 nm thick films of $Cs_2AgBiBr_6$ grown at 200 °C. (a) Absorptance from PDS measurements and Tauc plot (inset) displaying an estimated direct band gap of 2.24 eV. (b) PL centered at 1.90 eV and absorbance showing a distinct peak at 428 nm, characteristic to $Cs_2AgBiBr_6$.

2.24 eV direct band gap through a Tauc plot interpretation of the PDS data (Figure 5a), correlating well with values reported in literature. Longo et al.[3] reported a 2.25 eV direct band gap for sequentially evaporated thin films, and Slavney et al.[39] reported a 2.21 eV direct band gap for single crystals. PDS data also reveals a large density of subgap states, characteristic of $Cs_2AgBiBr_6$, and linked to nonradiative recombination in $Cs_2AgBiBr_6$ solar cell devices.[3] The PL peak, centered at 1.90 eV (653 nm), correlates well with reported values of 1.87 and 2.07 eV from single crystals and thin films, respectively.[3,39] Moreover, we observe a large Stokes shift between the main absorption edge and the PL emission. This effect has been widely reported in literature for $Cs_2AgBiBr_6$ films.[3,40] The absorbance peak at 2.90 eV (428 nm) is characteristic of $Cs_2AgBiBr_6$. Its origin is debated and assigned to either a tightly bound exciton or to a transition between Bi^{3+} electronic orbitals.[3,41,42]

Additionally, it is important to mention that the optimized PLD grown $Cs_2AgBiBr_6$ films, with no capping layer, were stored in a nitrogen glovebox and showed no sign of degradation, presenting the characteristic PL peak (Figure 5b) even after 1 year. Finally, the stability of the $Cs_2AgBiBr_6$ target used in this work was analyzed and showed little to no sign of degradation over 1 full year (Figure S8).

https://doi.org/10.1021/acs.chemmater.1c02054
Chem. Mater. 2021, 33, 7417−7422

IV. CONCLUSIONS

We have demonstrated the dry, single-step deposition of $Cs_2AgBiBr_6$ thin films by PLD, starting from a stoichiometric mixture of precursor powders, which were subsequently mechanochemically synthesized and pressed into solid targets with the $Cs_2AgBiBr_6$ phase. We demonstrate that tuning the deposition pressure and temperature allows for the fabrication of highly crystalline films of $Cs_2AgBiBr_6$. Films deposited at 200 °C show the formation of large crystalline grains with 200−300 nm sizes. The optical properties of these films also resemble those reported in literature for films deposited via sequential evaporation followed by annealing. This work emphasizes the potential to further explore PLD to deposit halide perovskite films with complex stoichiometries for a wide range of applications from light-emitting diodes, PV absorbers, UV, and X-ray detectors.

■ ASSOCIATED CONTENT

Supporting Information

The Supporting Information is available free of charge at https://pubs.acs.org/doi/10.1021/acs.chemmater.1c02054.

Detailed description of thermalization model, illustrative graphics, and additional XRD, SEM, and EDX analysis (PDF)

■ AUTHOR INFORMATION

Corresponding Author

Monica Morales-Masis − *MESA+ Institute for Nanotechnology, University of Twente, Enschede 7500 AE, The Netherlands;* orcid.org/0000-0003-0390-6839; Email: m.moralesmasis@utwente.nl

Authors

Nathan Rodkey − *MESA+ Institute for Nanotechnology, University of Twente, Enschede 7500 AE, The Netherlands; Insituto de Ciencia Molecular, Universidad de Valencia, 46980 Paterna, Spain;* orcid.org/0000-0003-4246-3911

Stan Kaal − *MESA+ Institute for Nanotechnology, University of Twente, Enschede 7500 AE, The Netherlands*

Paz Sebastia-Luna − *Insituto de Ciencia Molecular, Universidad de Valencia, 46980 Paterna, Spain;* orcid.org/0000-0001-6992-199X

Yorick A. Birkhölzer − *MESA+ Institute for Nanotechnology, University of Twente, Enschede 7500 AE, The Netherlands;* orcid.org/0000-0003-3133-2481

Martin Ledinsky − *Institute of Physics, Academy of Sciences of the Czech Republic, Prague 162 00, Czech Republic;* orcid.org/0000-0002-6586-5473

Francisco Palazon − *Insituto de Ciencia Molecular, Universidad de Valencia, 46980 Paterna, Spain;* orcid.org/0000-0002-1503-5965

Henk J. Bolink − *Insituto de Ciencia Molecular, Universidad de Valencia, 46980 Paterna, Spain;* orcid.org/0000-0001-9784-6253

Complete contact information is available at: https://pubs.acs.org/10.1021/acs.chemmater.1c02054

Notes

The authors declare no competing financial interest.

■ ACKNOWLEDGMENTS

The research leading to these results has received funding from the European Research Council (ERC) under the European Union's Horizon 2020 research and innovation program (Grant agreement Nos. 834431 and 852722), from SOLAR-ERA.NET Cofund 2 PERDRY. SOLAR-ERA.NET is supported by the European Comission within the EU Framework Programme for Research and Innovation HORIZON 2020 (Cofund ERA-NET Action, N° 786483), the Spanish Ministry of Science, Innovation and Universities, PCI2019-111829-2, CEX2019-000919-M, and FPU18/01732, and the Comunitat Valenciana IDIFEDER/2018/061, PROMETEU/2020/077. The authors acknowledge the support of the Operational Programme Research, Development, and Education financed by the European Structural and Investment Funds and the Czech Ministry of Education, Youth and Sports (Project Nos. CZ.02.1.01/0.0/0.0/16_019/0000760 SOLID21 and Czech-NanoLab Research Infrastructure LM2018110). The authors thank Guus Rijnders and Gertjan Koster at UT for helpful discussions regarding PLD growth, Kaijian Zhu and Annemarie Huijser for PL discussions, and Mark Smithers for SEM imaging.

■ REFERENCES

(1) Yang, B.; Pan, W.; Wu, H.; Niu, G.; Yuan, J. H.; Xue, K. H.; Yin, L.; Du, X.; Miao, X. S.; Yang, X.; Xie, Q.; Tang, J. Heteroepitaxial Passivation of $Cs_2AgBiBr_6$ Wafers with Suppressed Ionic Migration for X-Ray Imaging. *Nat. Commun.* **2019**, *10*, No. 1989.

(2) Chu, L.; Ahmad, W.; Liu, W.; Yang, J.; Zhang, R.; Sun, Y. Lead - Free Halide Double Perovskite Materials: A New Superstar Toward Green and Stable Optoelectronic Applications. *Nano-Micro Lett.* **2019**, *11*, No. 16.

(3) Longo, G.; Mahesh, S.; Buizza, L. R. V.; Wright, A. D.; Ramadan, A. J.; Abdi-Jalebi, M.; Nayak, P. K.; Herz, L. M.; Snaith, H. J. Understanding the Performance-Limiting Factors of $Cs_2AgBiBr_6$ Double-Perovskite Solar Cells. *ACS Energy Lett.* **2020**, *5*, 2200−2207.

(4) Lindquist, K. P.; Mack, S. A.; Slavney, A. H.; Leppert, L.; Gold-Parker, A.; Stebbins, J. F.; Salleo, A.; Toney, M. F.; Neaton, J. B.; Karunadasa, H. I. Tuning the Bandgap of $Cs_2AgBiBr_6$ through Dilute Tin Alloying. *Chem. Sci.* **2019**, *10*, 10620−10628.

(5) Bartel, C. J.; Sutton, C.; Goldsmith, B. R.; Ouyang, R.; Musgrave, C. B.; Ghiringhelli, L. M.; Scheffler, M. New Tolerance Factor to Predict the Stability of Perovskite Oxides and Halides. *Sci. Adv.* **2019**, *5*, No. eaav0693.

(6) Connor, B. A.; Biega, R. I.; Leppert, L.; Karunadasa, H. I. Dimensional Reduction of the Small-Bandgap Double Perovskite $Cs_2AgTlBr_6$. *Chem. Sci.* **2020**, *11*, 7708−7715.

(7) Wei, F.; Deng, Z.; Sun, S.; Hartono, N. T. P.; Seng, H. L.; Buonassisi, T.; Bristowe, P. D.; Cheetham, A. K. Enhanced Visible Light Absorption for Lead-Free Double Perovskite $Cs_2AgSbBr_6$. *Chem. Commun.* **2019**, *55*, 3721−3724.

(8) Khalfin, S.; Bekenstein, Y. Advances in Lead-Free Double Perovskite Nanocrystals, Engineering Band-Gaps and Enhancing Stability through Composition Tunability. *Nanoscale* **2019**, *11*, 8665−8679.

(9) Wang, C.; Liu, Y.; Guo, Y.; Ma, L.; Liu, Y.; Zhou, C.; Yu, X.; Zhao, G. Lead-Free Sodium Bismuth Halide Cs_2NaBiX_6 Double Perovskite Nanocrystals with Highly Efficient Photoluminescence. *Chem. Eng. J.* **2020**, *397*, No. 125367.

(10) Zhou, W.; Han, P.; Zhang, X.; Zheng, D.; Yang, S.; Yang, Y.; Luo, C.; Yang, B.; Hong, F.; Wei, D.; Lu, R.; Han, K. Lead-Free Small-Bandgap $Cs_2CuSbCl_6$ Double Perovskite Nanocrystals. *J. Phys. Chem. Lett.* **2020**, *11*, 6463−6467.

(11) Bekenstein, Y.; Dahl, J. C.; Huang, J.; Osowiecki, W. T.; Swabeck, J. K.; Chan, E. M.; Yang, P.; Alivisatos, A. P. The Making and Breaking of Lead-Free Double Perovskite Nanocrystals of Cesium

Silver-Bismuth Halide Compositions. *Nano Lett.* **2018**, *18*, 3502−3508.
(12) Wu, S.; Li, W.; Hu, J.; Gao, P. Antimony Doped Lead-Free Double Perovskites ($Cs_2NaBi_{1-x}Sb_xCl_6$) with Enhanced Light Absorption and Tunable Emission. *J. Mater. Chem. C* **2020**, *8*, 13603−13611.
(13) Gray, M. B.; Hariyani, S.; Strom, T. A.; Majher, J. D.; Brgoch, J.; Woodward, P. M. High-Efficiency Blue Photoluminescence in the $Cs_2NaInCl_6$:Sb^{3+} double Perovskite Phosphor. *J. Mater. Chem. C* **2020**, *8*, 6797−6803.
(14) Majher, J. D.; Gray, M. B.; Liu, T.; Holzapfel, N. P.; Woodward, P. M. Rb_3InCl_6: A Monoclinic Double Perovskite Derivative with Bright Sb^{3+} Activated Photoluminescence. *Inorg. Chem.* **2020**, *59*, 14478−14485.
(15) Greul, E.; Petrus, M. L.; Binek, A.; Docampo, P.; Bein, T. Highly Stable, Phase Pure $Cs_2AgBiBr_6$ Double Perovskite Thin Films for Optoelectronic Applications. *J. Mater. Chem. A* **2017**, *5*, 19972−19981.
(16) Daem, N.; Dewalque, J.; Lang, F.; Maho, A.; Spronck, G.; Henrist, C.; Colson, P.; Stranks, S. D.; Cloots, R. Spray-Coated Lead-Free $Cs_2AgBiBr_6$ Double Perovskite Solar Cells with High Open-Circuit Voltage. *Sol. RRL* **2021**, No. 2100422.
(17) Wu, C.; Zhang, Q.; Liu, Y.; Luo, W.; Guo, X.; Huang, Z.; Ting, H.; Sun, W.; Zhong, X.; Wei, S.; Wang, S.; Chen, Z.; Xiao, L. The Dawn of Lead-Free Perovskite Solar Cell: Highly Stable Double Perovskite $Cs_2AgBiBr_6$ Film. *Adv. Sci.* **2018**, *5*, No. 1700759.
(18) Miller, N. C.; Bernechea, M. Research Update: Bismuth Based Materials for Photovoltaics. *APL Mater.* **2018**, *6*, No. 084503.
(19) Burwig, T.; Guc, M.; Izquierdo-Roca, V.; Pistor, P. Synthesis and Crystal Structure Evolution of Co-Evaporated $Cs_2AgBiBr_6$ Thin Films upon Thermal Treatment. *J. Phys. Chem. C* **2020**, *124*, 9249−9255.
(20) Fan, P.; Peng, H.; Zheng, Z.; Chen, Z.; Tan, S.; Chen, X. Single-Source Vapor-Deposited Cs2AgBiBr6 Thin Films for Lead-Free Perovskite Solar Cells. *Nanomaterials* **2019**, *9*, No. 1760.
(21) Soto-Montero, T.; Soltanpoor, W.; Morales-Masis, M. Pressing Challenges of Halide Perovskite Thin Film Growth. *APL Mater.* **2020**, *8*, No. 110903.
(22) Palazon, F.; El Ajjouri, Y.; Bolink, H. J. Making by Grinding: Mechanochemistry Boosts the Development of Halide Perovskites and Other Multinary Metal Halides. *Adv. Energy Mater.* **2020**, *10*, No. 1902499.
(23) Li, K.; Xu, H.; Xu, Z.; Zeller, M.; Hunter, A. D. Semiconductive Coordination Networks from Bismuth(III) Bromide and 1,2-Bis-(Methylthio)Phenylacetylene-Based Ligands. *Inorg. Chem.* **2005**, *44*, 8855−8860.
(24) Tang, H.; Wang, Y.; Zhang, D.; Wu, K.; Huang, H. Shape-Controllable Synthesis and Morphology-Dependent Photocatalytic Properties of AgBr Photocatalysts. *J. Mater. Sci.: Mater. Electron.* **2016**, *27*, 6955−6963.
(25) Filip, M. R.; Hillman, S.; Haghighirad, A. A.; Snaith, H. J.; Giustino, F. Band Gaps of the Lead-Free Halide Double Perovskites $Cs_2BiAgCl_6$ and $Cs_2BiAgBr_6$ from Theory and Experiment. *J. Phys. Chem. Lett.* **2016**, *7*, 2579−2585.
(26) El Ajjouri, Y.; Chirvony, V. S.; Vassilyeva, N.; Sessolo, M.; Palazon, F.; Bolink, H. J. Low-Dimensional Non-Toxic $A_3Bi_2X_9$ Compounds Synthesized by a Dry Mechanochemical Route with Tunable Visible Photoluminescence at Room Temperature. *J. Mater. Chem. C* **2019**, *7*, 6236−6240.
(27) Tang, Y.; Liang, M.; Chang, B.; Sun, H.; Zheng, K.; Pullerits, T.; Chi, Q. Lead-Free Double Halide Perovskite Cs_3BiBr_6 with Well-Defined Crystal Structure and High Thermal Stability for Optoelectronics. *J. Mater. Chem. C* **2019**, *7*, 3369−3374.
(28) Tran, M. N.; Cleveland, I. J.; Aydil, E. S. Resolving the Discrepancies in the Reported Optical Absorption of Low-Dimensional Non-Toxic Perovskites, $Cs_3Bi_2Br_9$ and Cs_3BiBr_6. *J. Mater. Chem. C* **2020**, *8*, 10456−10463.
(29) Yang, J.; Zhang, P.; Wei, S. H. Band Structure Engineering of Cs2AgBiBr6 Perovskite through Order-Disordered Transition: A First-Principle Study. *J. Phys. Chem. Lett.* **2018**, *9*, 31−35.
(30) Ji, F.; Klarbring, J.; Wang, F.; Ning, W.; Wang, L.; Yin, C.; Figueroa, J. S. M.; Christensen, C. K.; Etter, M.; Ederth, T.; Sun, L.; Simak, S. I.; Abrikosov, I. A.; Gao, F. Lead-Free Halide Double Perovskite $Cs_2AgBiBr_6$ with Decreased Band Gap. *Angew. Chem.* **2020**, *132*, 15303−15306.
(31) Dijkkamp, D.; Venkatesan, T.; Wu, X. D.; Shaheen, S. A.; Jisrawi, N.; Min-Lee, Y. H.; McLean, W. L.; Croft, M. Preparation of Y-Ba-Cu Oxide Superconductor Thin Films Using Pulsed Laser Evaporation from High Tc Bulk Material. *Appl. Phys. Lett.* **1987**, *51*, 619−621.
(32) Liu, G. Z.; Lei, Q. Y.; Xi, X. X. Stoichiometry of $SrTiO_3$ Films Grown by Pulsed Laser Deposition. *Appl. Phys. Lett.* **2012**, *100*, No. 202902.
(33) Kiyek, V. M.; Birkhölzer, Y. A.; Smirnov, Y.; Ledinsky, M.; Remes, Z.; Momand, J.; Kooi, B. J.; Koster, G.; Rijnders, G.; Morales-Masis, M. Single-Source, Solvent-Free, Room Temperature Deposition of Black γ-$CsSnI_3$ Films. *Adv. Mater. Interfaces* **2020**, *7*, No. 2000162.
(34) Sturm, K.; Krebs, H. U. Quantification of Resputtering during Pulsed Laser Deposition. *J. Appl. Phys.* **2001**, *90*, 1061−1063.
(35) Westwood, W. D. Calculation of Deposition Rates in Diode Sputtering Systems. *J. Vac. Sci. Technol.* **1978**, *15*, 1−9.
(36) Li, J.; Gao, R.; Gao, F.; Lei, J.; Wang, H.; Wu, X.; Li, J.; Liu, H.; Hua, X.; Liu, S. F. Fabrication of Efficient $CsPbBr_3$ Perovskite Solar Cells by Single-Source Thermal Evaporation. *J. Alloys Compd.* **2020**, *818*, No. 152903.
(37) Patel, N.; Dias, S.; Krupanidhi, S. B. Vis-Near-Infrared Photodetectors Based on Methyl Ammonium Lead Iodide Thin Films by Pulsed Laser Deposition. *J. Electron. Mater.* **2018**, *47*, 2306−2315.
(38) Thornton, J. A. Influence of Apparatus Geometry and Deposition Conditions on the Structure and Topography of Thick Sputtered Coatings. *J. Vac. Sci. Technol.* **1974**, *11*, 666−670.
(39) Slavney, A. H.; Hu, T.; Lindenberg, A. M.; Karunadasa, H. I. A Bismuth-Halide Double Perovskite with Long Carrier Recombination Lifetime for Photovoltaic Applications. *J. Am. Chem. Soc.* **2016**, *138*, 2138−2141.
(40) Igbari, F.; Wang, R.; Wang, Z. K.; Ma, X. J.; Wang, Q.; Wang, K. L.; Zhang, Y.; Liao, L. S.; Yang, Y. Composition Stoichiometry of $Cs_2AgBiBr_6$ Films for Highly Efficient Lead-Free Perovskite Solar Cells. *Nano Lett.* **2019**, *19*, 2066−2073.
(41) Kentsch, R.; Scholz, M.; Horn, J.; Schlettwein, D.; Oum, K.; Lenzer, T. Exciton Dynamics and Electron-Phonon Coupling Affect the Photovoltaic Performance of the $Cs_2AgBiBr_6$ Double Perovskite. *J. Phys. Chem. C* **2018**, *122*, 25940−25947.
(42) Biega, R. I.; Filip, M. R.; Leppert, L.; Neaton, J. B. Chemically Localized Resonant Excitons in Silver-Pnictogen Halide Double Perovskites. *J. Phys. Chem. Lett.* **2021**, *12*, 2057−2063.

https://doi.org/10.1021/acs.chemmater.1c02054
Chem. Mater. 2021, 33, 7417−7422